Consecutive feedback-driven constitutional dynamic networks

Liang Yue[a], Shan Wang[a], Verena Wulf[a], Sivan Lilienthal[a], Françoise Remacle[b], R. D. Levine[a,1], and Itamar Willner[a,1]

[a]Institute of Chemistry, The Hebrew University of Jerusalem, 91904 Jerusalem, Israel; and [b]Theoretical Physical Chemistry, Research Unit Molecular Systems, University of Liege, 4000 Liege, Belgium

Contributed by R. D. Levine, December 29, 2018 (sent for review October 10, 2018; reviewed by Thomas Carell and Andrew J. Turberfield)

Cellular transformations are driven by environmentally triggered complex dynamic networks, which include signal-triggered feedback processes, cascaded reactions, and switchable transformations. We apply the structural and functional information encoded in the sequences of nucleic acids to construct signal-triggered constitutional dynamic networks (CDNs) that mimic the functions of natural networks. Using predesigned hairpin structures as triggers, the network generates functional strands, which stabilize one or the other of the constituents of the network, leading to feedback-driven reconfiguration and time-dependent equilibration of the networks. Using structurally designed hairpins, positive-feedback or negative-feedback mechanisms operated by the CDNs are demonstrated. With two predesigned hairpins, the coupled consecutive operations of negative/positive- or positive/positive-feedback cascades are accomplished. The time-dependent composition changes of the networks are well reproduced by chemical kinetics simulations that provide predictive behaviors of the network, under variable auxiliary conditions. Beyond mimicking natural network properties and functions by means of the synthetic nucleic-acid–based CDNs, the systems introduce versatile perspectives for the design of amplified sensors (sensing of miRNA-376a) and the development of logic gate circuits.

supramolecular chemistry | DNAzyme | biological regulation | systems chemistry | DNA hairpin

The central importance of feedback mechanisms in biological circuits has been clearly recognized since the discussion of the molecular mechanism in the pioneering work of Jacob and Monod (1, 2). Such circuits have been clearly identified in the regulation of gene transcription, in signal transduction, and in developmental networks (3–6). These circuits are often complemented by additional environmentally triggered events (7, 8). Extensive recent research efforts are being directed to the development of chemical networks mimicking functions of networks in nature (systems chemistry) (3–6). Significant progress toward this important goal is demonstrated with the assembly of dynamically equilibrated supramolecular mixtures by adapting equilibrated configurations and structures dictated by external, environmental triggers (9, 10). These include the assembly of constitutional dynamic networks (7, 11, 12), CDNs.

Nucleic acids provide versatile building blocks for the construction of CDNs due to the structural and functional information encoded in the biopolymer sequences (13–15). Diverse means to reversibly stabilize programmed nucleic acid structures were reported (16–20), and provide a rich "toolbox" for developing DNA switches (18, 21), machines (22, 23) and programmed structures (24, 25), and the area of DNA nanotechnology (26–28). Specifically, the triggered reconfiguration of DNA assemblies provides means to construct DNA-based CDNs and to dynamically equilibrate the CDNs by appropriate triggers (29–31).

In the present study, we introduce DNA-based feedback-driven CDNs. While the previous studies on nucleic-acid–based CDNs used an external trigger to stabilize one of the CDN constituents and to reconfigure the equilibrated states of the networks, the present study addresses the initiation of a time-dependent feedback mechanism that dynamically controls the contents of the constituents in the CDNs. That is, the feedback path provides an amplified transduction means to catalytically activate the constituents associated with the CDNs. In addition, we demonstrate that by applying two consecutive triggers, coupled negative/positive or positive/positive-feedback mechanisms proceed. Furthermore, kinetic simulations of the time-dependent control over the contents of the constituents in the CDNs allow us to fully mimic the kinetic behaviors of the CDNs, thus enabling a predictive guide to the feature of the CDNs under variable conditions. Fig. 1 depicts the principles for the assembly of such feedback-driven CDNs, consisting of four equilibrated constituents AA′, BB′, AB′, and BA′. While the pairs AA′/BB′ and AB′/BA′ do not share common components, the pairs AA′/AB′, AA′/BA′, BB′/AB′, and BB′/BA′ do share common components. As a result, the sharing of common components in the four constituents leads to an interconstituent equilibrated network. In fact, one may consider the constituents of the network as a "compass-poles" device composed of North (N)/South (S) directions and East (E)/West (W) directions corresponding to the equilibrated pairs that do not share common components, AA′ (N)/BB′ (S), and AB′ (E)/BA′ (W), respectively, as outlined for CDN "*X*." The triggered stabilization of any of the directions leads to the adaptive reequilibration of the respective CDN. This is exemplified in Fig. 1 with the dynamic feedback-driven adaptive reconfiguration of the parent CDN *X* with auxiliary triggers H_1 or H_2. Treatment of CDN *X* with H_1 results in the BB′-induced transformation of H_1 into E_1 that acts as a stabilization agent for AA′ (to form AA′-K^+).

Significance

Inspired by nature, where dynamic networks lead to adaptive compositions and emerging functions of the systems, we introduce nucleic-acid–based constitutional dynamic assemblies mimicking natural networks. We demonstrate that auxiliary triggers guide the adaptive reconfiguration of the compositions of the constitutional dynamic networks and their emerging functions. Specifically, we introduce the assembly of constitutional dynamic networks revealing negative/positive- and positive/positive-feedback–driven operation mechanisms. These processes mimic signal propagation phenomena in biological environments. The feedback-driven mechanisms provide the principles to develop dynamic amplified sensing platforms and to design cascaded logic gate circuits.

Author contributions: L.Y., S.W., and I.W. designed research; L.Y., S.W., V.W., S.L., F.R., R.D.L., and I.W. performed research; L.Y., S.W., and I.W. analyzed data; and L.Y., S.W., V.W., R.D.L., and I.W. wrote the paper.

Reviewers: T.C., Ludwig Maximilians University; and A.J.T., University of Oxford.

The authors declare no conflict of interest.

[1]To whom correspondence may be addressed. Email: rafi@fh.huji.ac.il or willnea@vms.huji.ac.il.

This article contains supporting information online at www.pnas.org/lookup/suppl/doi:10.1073/pnas.1816670116/-/DCSupplemental.

Published online February 6, 2019.

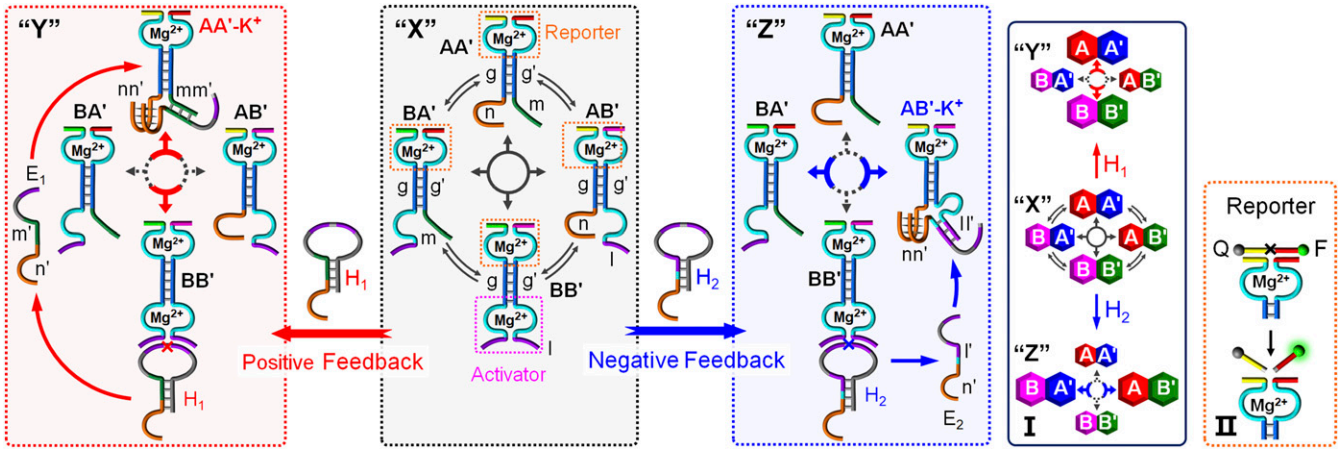

Fig. 1. Schematic dynamic feedback-driven adaptive reconfiguration of CDN *X*. Transition of CDN *X* into CDN *Y*: positive-feedback–driven dynamic equilibration of CDN *X* via the cleavage of hairpin H_1 by the DNAzyme activator associated with BB′, and the stabilization of the constituent AA′ with E_1 through the formation of a K^+-ion–stabilized G quadruplex (AA′-K^+). Transition of CDN *X* into CDN *Z*: negative-feedback–driven equilibration of CDN *X* via the cleavage of H_2 by BB′, and the stabilization of AB′ with E_2 through the formation of a K^+-ion–stabilized G quadruplex (AB′-K^+). (*Inset I*) The adaptive triggered transitions across the networks are displayed in the form of dynamic equilibration of four constituents that follow a compass-poles device (see text). The constituents are displayed in the form of interequilibration dimer titles. (*Inset II*) Schematic readout of the performances of the CDNs by the application of four different Mg^{2+}-ion–dependent DNAzymes as reporters.

The stabilization of AA′ results in its up-regulation, the concomitant up-regulation of BB′, and the down-regulation of AB′ and BA′. The up-regulation of the activator BB′ leads to a faster transformation of H_1 into E_1, resulting in the positive-feedback–driven adaptive reconfiguration of CDN *X* into "*Y*." In a complementary manner, treatment of CDN *X* with H_2 results in the BB′-stimulated generation of E_2 that stabilizes AB′ (to form AB′-K^+). As a result, AB′ and BA′ are up-regulated, while AA′ and the activator BB′ are down-regulated. That is, the time-dependent BB′-induced formation of E_2 leads to a negative-feedback–driven adaptive transition of CDN *X* into "*Z*."

Fig. 1 outlines the principles for the feedback-driven reequilibration of the different CDNs. A major challenge while investigating these CDNs is, however, the development of analytical means to follow and confirm the quantitative contents of the constituents in the different CDNs. This is accomplished by the functionalization of each of the constituents with a different Mg^{2+}-ion–dependent DNAzyme that includes specific "arms" for the recognition and cleavage of a specific fluorophore/quencher-modified substrate. The DNAzyme sites act as reporter units for the quantitative assessment of the contents of the respective constituents by following the fluorescence intensities of the cleaved-off substrates and using appropriate calibration curves (Fig. 1, *Inset II*). The quantitative evaluation of the equilibrated contents is further achieved by quantitative imaging of electrophoretically separated and stained bands.

Results

Positive-Feedback–Driven Dynamic Equilibration of CDN *X*. Fig. 1 shows schematically the composition of CDN *X* that stimulates a dynamically driven feedback mechanism. The system includes four equilibrated constituents AA′, AB′, BA′, and BB′. To each of the constituents, a **gg′** dynamic hybridization domain and a specific Mg^{2+}-ion–dependent DNAzyme subunit (*SI Appendix*, Fig. S1) are integrated. These DNAzyme units act as reporters for the feedback-driven operation of the CDN. BB′ includes an additional Mg^{2+}-ion–dependent DNAzyme unit as an activator to initiate the feedback process. AA′ is further functionalized with two single-stranded tethers **n** and **m**, where **n** consists of a guanosine-rich domain, a functional subunit for the formation of a G quadruplex (*SI Appendix*, Fig. S1). CDN *X* is subjected to hairpin H_1 triggering the initiation of the positive-feedback process. H_1 includes, in its loop region, a ribonucleobase sequence that is recognized by the activator DNAzyme subunit of BB′, and contains the sequences **n′** and **m′** partially caged in the hairpin stem. In the presence of Mg^{2+} ions, H_1 is cleaved, yielding the fragmented strand E_1 that includes **n′** and **m′**. The sequence **n′** is a guanosine-rich sequence, a subunit for the formation of a G quadruplex, while **m′** is complementary to **m** associated with AA′. That is, the cleavage of H_1 by BB′ yields E_1 that binds to AA′ through the formation of a K^+-ion–stabilized G quadruplex (**nn′**) and the cooperative stabilization by duplex **mm′**. The binding of E_1 to AA′ results in its enrichment at the expense of AB′ and BA′, and a concomitant increase in BB′. The enrichment of BB′ results, however, in the enhancement of the cleavage of H_1 and the dynamical enrichment of AA′ that further increases the content of BB′. That is, by the appropriate design of the system, a time-dependent positive-feedback mechanism is driven by the CDN. This feedback mechanism proceeds as long as H_1 is available.

Fig. 2*A* depicts the cleavage rates of the respective substrates by the constituents AA′, BB′, BA′, and AB′ before (*i*) and after (*ii*) subjecting CDN *X* to hairpin H_1 for 24 h. The cleavage rates of AA′ and BB′ increase upon the addition of H_1, whereas the cleavage rates of BA′ and AB′ decrease, reflecting changes in the concentrations of the respective constituents. (Note that the equilibria of the CDNs are not affected by the binding of the substrates, *SI Appendix*, Fig. S2.) Using the appropriate calibration curves (*SI Appendix*, Fig. S3), we quantitatively analyzed the concentrations of the constituents before and after interacting with H_1 (Table 1). After interaction of CDN *X* with H_1, the contents of AA′ and BB′ increase by 78% and 72%, respectively, whereas the contents of BA′ and AB′ decrease by 46% and 49%. These concentration changes were further supported by quantitative gel electrophoresis experiments (Table 1 and *SI Appendix*, section I and Fig. S4). We find that the concentration changes of the constituents in the CDN are slow compared with the cleavage rates of the substrates by the DNAzyme reporters. This allows us to monitor the compositions of the CDN at different time intervals until it reaches the final equilibrium. The catalyzed cleavage rates of the substrates associated with AA′ and BB′ increase and those associated with BA′ and AB′ decrease during the feedback-driven equilibration of CDN *X* (*SI Appendix*, Fig. S5). Fig. 2*B* shows the quantitative

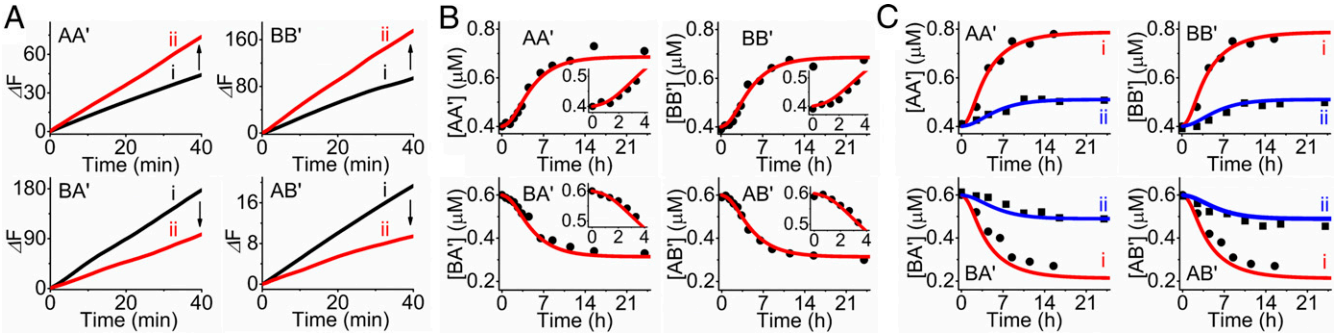

Fig. 2. Positive-feedback–driven dynamic equilibration of CDN *X*. (*A*) Catalytic activities of the DNAzyme reporter units associated with the constituents of the CDN: (*i*) Before and (*ii*) after treatment of CDN *X* with H_1 for 24 h. (*B*) Computationally simulated (solid curves) and experimentally determined (dots) time-dependent concentration changes of the constituents of the CDN upon subjecting CDN *X* to H_1, 2 μM. (*Insets*) Nonlinear, concentration changes of the constituents at short time intervals. (*C*) Computationally predicted (solid curves) and experimentally determined (dots) time-dependent concentration changes of the constituents of the CDN upon subjecting CDN *X* to H_1 with different concentrations: (*i*) 5 μM and (*ii*) 0.5 μM.

concentrations of the constituents at different time intervals during equilibration of CDN *X*. Evidently, the contents of AA′ and BB′ increase nonlinearly within a time interval of ∼10 h until they reach saturation. Concomitantly, a nonlinear decrease in the contents of BA′ and AB′ within this time interval is observed. Control experiments reveal that in the absence of K^+ ions, no concentration changes are observed (*SI Appendix*, Fig. S6), implying that the K^+-ion–stabilized G quadruplex associated with AA′ is, indeed, responsible for the reequilibration of CDN *X*. The K^+-ion–stabilized G-quadruplex–driven feedback mechanism was further supported by following the activity of the hemin/G-quadruplex DNAzyme associated with AA′-K^+, *SI Appendix*, section II and Fig. S7. Knowing the concentration changes of the constituents of CDN *X* during its reequilibration after the addition of H_1 and approximate cleavage-rate constants of Mg^{2+}-ion–dependent DNAzymes, we computationally simulated the time-dependent concentration changes of the constituents upon triggering CDN *X* with H_1. A set of differential equations following the kinetic profile of the positive-feedback–driven process outlined in Fig. 1 was formulated and is provided in *SI Appendix*, section III. The fitting procedure yielded the set of rate constants given in *SI Appendix*, Table S1. A very good fit for the time-dependent concentration changes of all constituents using this set of rate constants is observed (Fig. 2*B*, solid curves). The kinetic simulation of the experimental results has, however, a value, only if the set of reaction rate constants involved in the kinetic scheme has the predictive power to evaluate kinetic features of CDN *X* subjected to other auxiliary conditions, which can be subsequently verified by experiments. Accordingly, the concentration of H_1 (2 μM) was changed to 5 or 0.5 μM. Using the set of derived reaction rate constants, the computationally simulated concentration changes of the constituents upon subjecting the CDN to H_1, 5 or 0.5 μM, are presented in Fig. 2*C* (solid curves). Excellent agreements between the predicted time-dependent concentration changes and the experimental results (dots in Fig. 2*C*, derived from *SI Appendix*, Figs. S8 and S9) are demonstrated. (It should be noted that the experiments were performed after the generation of the computationally simulated results.) These results imply that the set of rate constants derived from the initial simulations can predict the performance of the operation of feedback-driven CDNs under different conditions.

Table 1. Initial and final concentrations of the constituents in the CDNs driven by the positive-feedback mechanism and the negative-feedback mechanism (Fig. 1)

System	Concentration, μM			
	[AA′]	[AB′]	[BA′]	[BB′]
Positive-feedback–driven CDN in Fig. 1				
(*i*)*	0.40	0.59	0.61	0.39
(*i*)†	(0.45)	(0.65)	(0.64)	(0.40)
(*ii*)*	0.71	0.30	0.33	0.67
(*ii*)†	(0.68)	(–)‡	(–)‡	(0.74)
Negative-feedback–driven CDN in Fig. 1				
(*iii*)*	0.40	0.59	0.61	0.39
(*iii*)†	(0.43)	(0.65)	(0.62)	(0.43)
(*iv*)*	0.19	0.77	0.80	0.19
(*iv*)†	(0.25)	(0.82)	(0.81)	(0.20)

(*i*) Before the application of H_1; (*ii*) After the application of H_1 (24 h); (*iii*) Before the application of H_2; (*iv*) After the application of H_2 (24 h).
*Concentration data provided by the DNAzyme reporter units.
†Concentration data extracted by quantitative analysis of the electrophoretically separated stained bands.
‡Concentrations cannot be evaluated owing to the overlap of the bands.

Several complementary control experiments reveal the significance of the catalytic cleavage of H_1 by BB′ to stimulate the operation of the feedback mechanism leading to the reequilibration of CDN *X*. Subjecting CDN *X* to a non–ribonucleobase-containing (noncleavable) hairpin H_1*, no content changes of the constituents are observed, implying that the cleavage of H_1 is essential to induce the reequilibration of the CDN (*SI Appendix*, Fig. S10). Further, H_1 was mutated to yield H_1^m, where the stem domain is not altered, whereas in the **m′** domain of the hairpin loop, a guanine base is exchanged by a cytosine base. Under this condition, the cleaved-off strand E_1^m includes a C-C mismatch that prohibits the cooperative duplex **mm′** stabilization of the G quadruplex. These results confirm that the cooperative stabilization of the G quadruplex by **mm′** is essential to operate the feedback-driven process (*SI Appendix*, Fig. S11). However, upon subjecting CDN *X* directly to E_1, in the absence of H_1, a monotonic increase in the contents of AA′ and BB′, and a concomitant monotonic decrease in the contents of BA′ and AB′ are observed (*SI Appendix*, Fig. S12). That is, the induction time interval required to initiate the feedback mechanism by cleaving H_1 is absent in the presence of the "pure" E_1. It should be noted that the final equilibrated contents of the constituents generated by the positive-feedback–driven mechanism or by the direct addition of the effector unit E_1 are similar. Nonetheless, we note that while the feedback-driven process involves a dynamic time-dependent evolution of the E_1-guided equilibrated system, the instantaneous addition of E_1 to the system represents a trigger event. Naturally, the kinetics for the formation of the equilibrated state, by the two mechanisms, are different. The feedback-driven process reveals, as expected, a nonlinear kinetic evolution of the

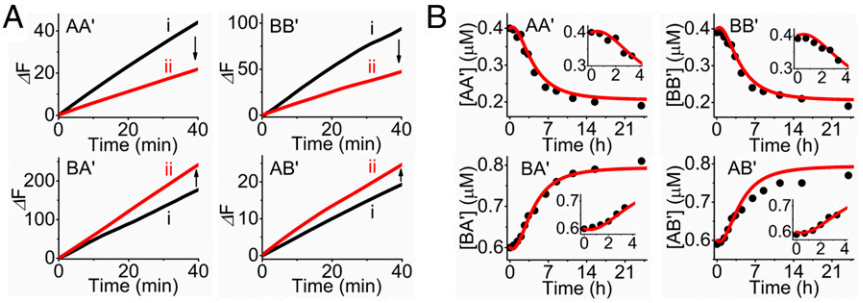

Fig. 3. Negative-feedback–driven dynamic equilibration of CDN *X*. (*A*) Catalytic activities of the DNAzyme reporter units associated with the constituents of the CDN: (*i*) Before and (*ii*) after subjecting CDN *X* to H_2 for 24 h. (*B*) Computationally simulated (solid curves) and experimentally determined (dots) time-dependent concentration changes of the constituents of the CDN upon treatment of CDN *X* with H_2. (*Insets*) Nonlinear, concentration changes of the constituents at short time intervals.

equilibrated CDNs. For further evaluation of the effect of changes in the initial contents of the equilibrated constituents of CDN *X* (by introducing mutation in BA′) on the positive-feedback mechanism, see *SI Appendix*, section IV, Figs. S13–S15, and Table S2.

Negative-Feedback–Driven Dynamic Equilibration of CDN *X*. The orthogonal feedback-driven transformation of CDN *X* into *Z* is shown in Fig. 1. In this system, CDN *X* is subjected to a different hairpin H_2 that is cleaved by BB′ to yield the fragmented strand E_2 including the sequences **n**′ and **l**′. This strand forms, in the presence of K^+ ions, a G quadruplex, with AB′, in which the G quadruplex is synergistically stabilized by the duplex **ll**′. The stabilization of AB′ is then anticipated to up-regulate AB′ and BA′ and concomitantly down-regulate AA′ and BB′. The positive-feedback mechanism discussed in Fig. 1 reveals the time-dependent increase in the concentration of the activator BB′, which is responsible for cutting the hairpin trigger, until reaching the new equilibrium. In contrast, subjecting CDN *X* to H_2 leads to the time-dependent decrease in the content of BB′. This decrease is thus defined as a negative-feedback–driven reequilibration of the CDN.

Fig. 3*A* shows the time-dependent fluorescence changes generated by the constituents of the CDN, before (*i*) and after (*ii*) subjecting CDN *X* to H_2 for 24 h. Using appropriate calibration curves (*SI Appendix*, Fig. S3), we find that the increases in the contents of BA′ and AB′ correspond to 31% and 31%, while the contents of AA′ and BB′ decrease by 53% and 51%, respectively (Table 1). These data were further supported by quantitative gel electrophoresis experiments (Table 1 and *SI Appendix*, section V and Fig. S16). The H_2-driven reequilibration of CDN *X* is a dynamic, time-dependent process. From the cleavage rates of the substrates by the respective constituents at different time intervals during equilibration of the system (*SI Appendix*, Fig. S17), we derived the time-dependent concentration changes of the constituents, Fig. 3*B*. The results reveal, as before, an initial induction time of ~2 h, in which the concentration changes of the constituents are very small (Fig. 3*B*, *Insets*). This induction time is accompanied by a sharp increase in the concentration changes of the constituents that proceeds within 3–4 h, and subsequently small concentration changes leading to the equilibration of the new CDN state. As before, the negative-feedback–driven CDN was computationally simulated, and the results are presented as solid curves overlaying the experimental data (dots), Fig. 3*B* (for more details see *SI Appendix*, section VI and Table S3). Control experiments reveal that, in the absence of K^+ ions, no concentration changes are observed (*SI Appendix*, Fig. S18), implying that the K^+-ion–stabilized G quadruplex, AB′-K^+, is, indeed, responsible for the reequilibration of CDN *X*. We note that the final equilibrated contents of the constituents generated by the negative-feedback–driven mechanism or by the direct addition of the effector E_2 are similar, *SI Appendix*, Fig. S19. The rates of the formation of the equilibrated state by the two paths are different. While the instantaneous addition of E_2 provides a trigger event that leads to a rapid transformation of CDN *X* into *Z*, the time-dependent evolution of E_2 through the cleavage of H_2 leads to a dynamic nonlinear formation of the equilibrated CDN *Z*. For further evaluation of the effect of changes in the initial contents of the equilibrated constituents of CDN *X* (by introducing mutation in AA′) on the negative-feedback–driven reequilibration of the CDN in the presence of H_2 see *SI Appendix*, section VII, Figs. S20–S22, and Table S2.

Negative/Positive-Feedback–Driven Equilibration of CDN "*R*." The ability to control the CDN by two different triggers yielding positive- or negative-feedback mechanisms and the dynamic feedback-driven equilibration of the CDN provides a means to stimulate cascaded negative/positive- or positive/positive-feedback mechanisms. Fig. 4*A* presents the design of CDN *R* that performs a sequential equilibration cascade involving a negative/positive-feedback path. CDN *R* includes the constituents CC′, DD′, CD′, and DC′. Each of the constituents contains a duplex-bridged structure separated by two single-stranded loops (the loop sequences are different in the constituents!). To each of the

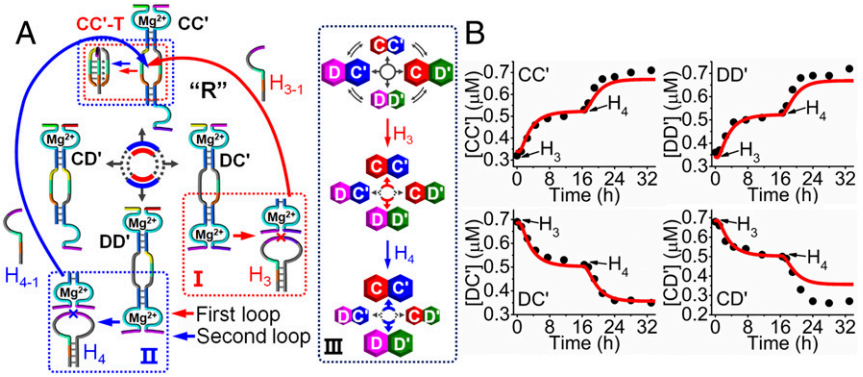

Fig. 4. Biphase negative/positive-feedback–driven dynamic equilibration of CDN *R*. (*A*) Bimodal operation of CDN *R* using two consecutive negative/positive-feedback processes, using triggers H_3 and H_4, presented schematically in the form of a compass-poles device. The stepwise reconfigured equilibrated compositions of the CDN in the negative/positive-feedback mechanism are schematically presented (*Right*) in the form of different sized blockers of the up-regulated and down-regulated constituents. (*B*) Computationally simulated (solid curves) and experimentally determined (dots) time-dependent concentration changes of the CDN constituents upon biphase negative/positive-feedback operation.

Table 2. Initial and final concentrations of the constituents in the CDNs driven by the negative/positive-feedback mechanism (Fig. 4*A*) and the positive/positive-feedback mechanism (Fig. 5*A*)

System	Concentration, μM [CC′]	[CD′]	[DC′]	[DD′]
Negative/positive-feedback system in Fig. 4*A*				
(*i*)*	0.32	0.69	0.68	0.36
(*i*)†	(0.32)	(0.74)	(0.70)	(0.30)
(*ii*)*	0.53	0.50	0.51	0.53
(*ii*)†	(0.48)	(0.44)	(0.51)	(0.47)
(*iii*)*	0.71	0.27	0.35	0.72
(*iii*)†	(0.74)	(0.30)	(0.34)	(0.75)
Positive/positive-feedback system in Fig. 5*A*				
(*iv*)*	0.57	0.41	0.42	0.61
(*iv*)†	(0.64)	(0.28)	(0.35)	(0.67)
(*v*)*	0.37	0.71	0.73	0.32
(*v*)†	(0.32)	(0.66)	(0.65)	(0.34)

(*i*) CDN *R* before the application of any hairpins; (*ii*) After subjecting CDN *R* to H_3 (16.5 h); (*iii*) After subjecting the resulting CDN (*ii*) to H_4 for additional 16.5 h; (*iv*) After subjecting CDN *R* to H_4 (16.5 h); (*v*) After subjecting the resulting CDN (*iv*) to H_5 for additional 16.5 h.

*Concentration data provided by the DNAzyme reporter units.

†Concentration data extracted from quantitative analysis of the electrophoretically separated stained bands.

constituents, a different DNAzyme reporter unit is conjugated. In addition, DC′ and DD′ include an additional DNAzyme unit activating and controlling the feedback-driven equilibration of CDN *R*, respectively, in the presence of appropriate hairpin triggers. Subjecting CDN *R* to hairpin trigger H_3 leads to its cleavage by DC′. The cleaved-off strand H_{3-1} hybridizes with the double-loop region of CC′ to yield a T-A·T triplex that stabilizes CC′ (CC′-T; for details see *SI Appendix*, Fig. S23). This stabilization enriches CC′ at the expense of CD′ and DC′, and DD′ is enriched concomitantly, resulting in a dynamic, time-dependent, negative-feedback–driven process. After the completion of the first feedback-driven equilibration loop evidenced by a saturated composition of the equilibrated mixture, hairpin H_4 is introduced and cleaved by the DNAzyme activator associated with DD′. The cleavage of H_4 yields the strand H_{4-1} that further interacts with the vacant double-loop domain of CC′. This results in the further enrichment of CC′, leading to a secondary, dynamic, positive-feedback–driven process where DD′ is enriched and concomitantly CD′ and DC′ are down-regulated. That is, the cleavage of H_4 and the formation of H_{4-1} activate the second feedback-driven loop and shift the equilibrium of the system.

Upon the stepwise treatment of CDN *R* with H_3 and H_4, the cleavage rates indicate a stepwise increase in CC′ and DD′ and a decrease in DC′ and CD′ (*SI Appendix*, Fig. S24). Using the appropriate calibration curves (*SI Appendix*, Fig. S25), the time-dependent, negative/positive-feedback–driven concentration changes of the constituents are derived (Fig. 4B). Evidently, a stepwise increase in the contents of CC′ (66% and 59%) and DD′ (47% and 53%), and a concomitant decrease in the contents of DC′ (25% and 25%) and CD′ (28% and 33%) are observed. Further support for these concentration changes was obtained by quantitative gel electrophoresis experiments (*SI Appendix*, section VIII and Fig. S26). A very good agreement of the concentrations of the constituents derived by the activities of DNAzyme reporter units and by the electrophoretic imaging is demonstrated (Table 2).

Positive/Positive-Feedback–Driven Equilibration of CDN *R*. The results shown in Fig. 4 represent a two-step negative/positive-feedback–driven equilibration of CDN *R*. One may, however, design a sequential positive/positive-feedback mechanism triggered by two hairpins, H_4 and H_5, as outlined in Fig. 5*A*. Triggering CDN *R* (identical to that outlined in Fig. 4*A*) with H_4 results in the dynamically driven positive-feedback equilibration of CDN *R*, whereby a time-dependent concentration increase of CC′ and DD′ takes place with a concomitant decrease of DC′ and CD′. In the second loop, applying the resulting CDN to H_5, the cleavage of H_5 yields the fragmented H_{5-1} that is designed to form a T-A·T triplex with the double-loop domain of CD′. The stabilization of CD′ results in an opposite positive-feedback–driven equilibration process, in which a dynamic time-dependent concentration increase of CD′ and DC′, and a concomitant decrease of CC′ and DD′, proceed. That is, while in the first feedback loop of CDN *R*, a dynamically driven, time-dependent increase in CC′ and DD′ occurs, the contents of the same constituents are down-regulated during the second feedback loop. Upon the stepwise interaction of CDN *R* with H_4 and H_5, the cleavage rates indicate a stepwise increase/decrease in CC′ and DD′ and a decrease/increase in DC′ and CD′ (*SI Appendix*, Fig. S27). Using the respective calibration curves (*SI Appendix*, Fig. S25), the time-dependent concentration changes of the constituents during the reconfiguration of CDN *R* were evaluated, Fig. 5*B*. The treatment of CDN *R* with H_4 yields a time-dependent, positive-feedback–driven increase in the contents of CC′ and DD′ (by 78% and 69%, respectively) and the parallel decrease in the contents of DC′ and CD′ (by 38% and 41%, respectively). Treatment of the resulting CDN with H_5 (time marked with arrow) leads to the down-regulation of CC′ and DD′ (by 35% and 48%, respectively) and to the up-regulation of DC′ and CD′ (by 74% and 73%, respectively). The up-regulation and subsequent down-regulation of CC′ and DD′ represents a triggered switchable behavior of the feedback process. Further support for these concentration changes was obtained by quantitative gel electrophoresis (*SI Appendix*, section IX and Fig. S28). The two methods (DNAzyme

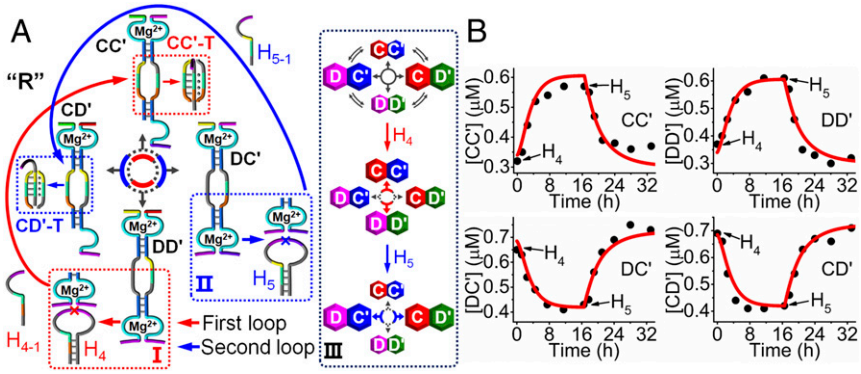

Fig. 5. Sequential positive/positive-feedback–driven dynamic equilibration of CDN *R*. (*A*) Bimodal operation of CDN *R* using two consecutive positive/positive-feedback processes, applying triggers H_4 and H_5, presented schematically in the form of a compass-poles device. The stepwise reconfigured equilibrated concentrations of the constituents in the positive/positive-feedback mechanism are schematically presented (*Right*) in the form of different sized blockers of the up-regulated and down-regulated constituents. (*B*) Computationally simulated (solid curves) and experimentally determined (dots) time-dependent concentration changes of the constituents of CDN *R* upon biphase positive/positive-feedback operation.

reporters and electrophoretic imaging) provide comparable values (Table 2). In addition, the stepwise negative/positive-feedback–driven CDN using H_3 and H_4, and the positive/positive-feedback–driven CDN triggered by H_4 and H_5 were computationally simulated. The overlaid computationally simulated time-dependent concentration changes of the constituents on the experimental data are presented in Figs. 4*B* and 5*B* (solid curves), respectively. (For the set of the differential equations and rate constants see *SI Appendix*, sections X and XI and Tables S4 and S5.)

Discussion

The present study has introduced the important element of dynamic feedback into nucleic-acid–based CDNs. We demonstrate that by the appropriate design of the constituents comprising the networks, programmed positive or negative-feedback–driven CDN systems are generated. Furthermore, we show that by subjecting the CDNs to dual triggers, negative/positive or positive/positive-feedback responses are possible. Beyond enhancing the complexity of nucleic-acid–based networks, we introduce several features inspired by nature: (*i*) The systems adapt themselves and respond to external triggers. Specifically, we introduce the K^+-ion stabilization of G-quadruplex structures and the strand-induced formation of T-A·T triplexes as motives stabilizing predesigned CDN constituents. (*ii*) Stabilization of one of the CDN constituents leads to the initiation of the respective feedback mechanism. The single-step feedback process represents a signal amplification process and a signal transduction mechanism that amplifies and catalytically activates the constituent that is agonistic to the energetically stabilized constituent. (*iii*) By applying two consecutive triggers, coupled negative/positive and positive/positive-feedback mechanisms were designed. These processes represent information transfer between constituents, mimicking signal propagation in biological networks. Note, however, that beyond the demonstration that nucleic-acid–based feedback-driven CDNs mimic biological systems, the feedback processes represent signal-triggered amplification paths. Thus, the CDNs-stimulated feedback mechanisms may provide versatile means to develop amplified sensor systems. This is exemplified in *SI Appendix*, section XII and Figs. S29 and S30 with the development of a CDN for the analysis of miRNA-376a, a biomarker for hepatocellular carcinoma. (*iv*) Furthermore, we note that the feedback-driven process made use of a fragmented hairpin strand that acts as a trigger. Nonetheless, the formation of the feedback trigger is accompanied by the generation of an "unused" strand. This strand can be used, in principle, as an activator of cascaded networks, being a potential source for generating feedback cascades. (*v*) The experimental time-dependent concentration changes of the constituents in the different CDNs were computationally simulated. The kinetic modeling of the CDNs and the obtained set of reaction rate constants, provide a versatile tool to predict the behavior of the CDNs subjected to different concentrations of the hairpin triggers.

Materials and Methods

Preparation of CDN *X*. CDN *X*, including the constituents AA′, AB′, BA′, and BB′, was prepared as follows: A mixture of A, B, A′, B′, 2 μM each, in Hepes buffer 10 mM, pH = 7.2, which includes $MgCl_2$ (20 mM) and KCl (50 mM), was annealed at 65 °C, cooled down to 25 °C at a rate of 0.33 °C min^{-1}, and allowed to equilibrate for 2 h at 25 °C.

Probing the Feedback-Driven CDNs by Catalytic Functions of the CDNs (Fig. 1). Taking the positive-feedback system as an example, CDN *X*, each component 1 μM, was subjected to H_1, 2 μM, in Hepes buffer 10 mM, pH = 7.2, which includes $MgCl_2$ (20 mM) and KCl (50 mM) and allowed to equilibrate at 28 °C. At different time intervals, aliquots of 60 μL were withdrawn from the mixture, and treated with the substrates, sub1 for AA′, sub2 for BB′, sub3 for BA′, sub4 for AB′, 3 μL of 100 μM each. The time-dependent fluorescence changes driven by the cleavage of the different substrates by the respective catalytic constituents were followed.

For more detailed materials, methods, and kinetic equations used for simulations please see *SI Appendix*.

ACKNOWLEDGMENTS. This research is supported by Israel Science Foundation and Minerva Center for Biohybrid Complex Systems. F.R. thanks Fonds National de la Recherche Scientifique, Belgium, for its support.

1. Jacob F, Monod J (1961) Genetic regulatory mechanisms in the synthesis of proteins. *J Mol Biol* 3:318–356.
2. Thomas R, D'Ari R (1990) *Biological Feedback* (CRC Press, Boca Raton, FL).
3. Alon U (2007) Network motifs: Theory and experimental approaches. *Nat Rev Genet* 8:450–461.
4. Herrmann A (2014) Dynamic combinatorial/covalent chemistry: A tool to read, generate and modulate the bioactivity of compounds and compound mixtures. *Chem Soc Rev* 43:1899–1933.
5. Corbett PT, et al. (2006) Dynamic combinatorial chemistry. *Chem Rev* 106:3652–3711.
6. Ashkenasy G, Hermans TM, Otto S, Taylor AF (2017) Systems chemistry. *Chem Soc Rev* 46:2543–2554.
7. Lehn JM (2015) Perspectives in chemistry–Aspects of adaptive chemistry and materials. *Angew Chem Int Ed Engl* 54:3276–3289.
8. Vantomme G, Jiang S, Lehn JM (2014) Adaptation in constitutional dynamic libraries and networks, switching between orthogonal metalloselection and photoselection processes. *J Am Chem Soc* 136:9509–9518.
9. Giuseppone N, Lehn JM (2004) Constitutional dynamic self-sensing in a zinc(II)/polyiminofluorenes system. *J Am Chem Soc* 126:11448–11449.
10. Au-Yeung HY, Cougnon FBL, Otto S, Pantos GD, Sanders JKM (2010) Exploiting donor–acceptor interactions in aqueous dynamic combinatorial libraries: Exploratory studies of simple systems. *Chem Sci* 1:567–574.
11. Holub J, Vantomme G, Lehn JM (2016) Training a constitutional dynamic network for effector recognition: Storage, recall, and erasing of information. *J Am Chem Soc* 138: 11783–11791.
12. Giuseppone N, Schmitt JL, Lehn JM (2004) Generation of dynamic constitutional diversity and driven evolution in helical molecular strands under Lewis acid catalyzed component exchange. *Angew Chem Int Ed Engl* 43:4902–4906.
13. Wang F, Lu CH, Willner I (2014) From cascaded catalytic nucleic acids to enzyme-DNA nanostructures: Controlling reactivity, sensing, logic operations, and assembly of complex structures. *Chem Rev* 114:2881–2941.
14. Gines G, et al. (2017) Microscopic agents programmed by DNA circuits. *Nat Nanotechnol* 12:351–359.
15. Genot AJ, et al. (2016) High-resolution mapping of bifurcations in nonlinear biochemical circuits. *Nat Chem* 8:760–767.
16. Hu Y, Cecconello A, Idili A, Ricci F, Willner I (2017) Triplex DNA nanostructures: From basic properties to applications. *Angew Chem Int Ed Engl* 56:15210–15233.
17. Lu CH, et al. (2013) Switchable catalytic acrylamide hydrogels cross-linked by hemin/G-quadruplexes. *Nano Lett* 13:1298–1302.
18. Kamiya Y, Asanuma H (2014) Light-driven DNA nanomachine with a photoresponsive molecular engine. *Acc Chem Res* 47:1663–1672.
19. Zhang DY, Turberfield AJ, Yurke B, Winfree E (2007) Engineering entropy-driven reactions and networks catalyzed by DNA. *Science* 318:1121–1125.
20. Davis JT, Spada GP (2007) Supramolecular architectures generated by self-assembly of guanosine derivatives. *Chem Soc Rev* 36:296–313.
21. Wang F, Liu X, Willner I (2015) DNA switches: From principles to applications. *Angew Chem Int Ed Engl* 54:1098–1129.
22. Bath J, Turberfield AJ (2007) DNA nanomachines. *Nat Nanotechnol* 2:275–284.
23. Seeman NC (2005) From genes to machines: DNA nanomechanical devices. *Trends Biochem Sci* 30:119–125.
24. Chidchob P, Sleiman HF (2018) Recent advances in DNA nanotechnology. *Curr Opin Chem Biol* 46:63–70.
25. Douglas SM, Bachelet I, Church GM (2012) A logic-gated nanorobot for targeted transport of molecular payloads. *Science* 335:831–834.
26. Seeman NC, Sleiman HF (2017) DNA nanotechnology. *Nat Rev Mater* 3:17068.
27. Seeman NC (2007) An overview of structural DNA nanotechnology. *Mol Biotechnol* 37:246–257.
28. Lu CH, Willner B, Willner I (2013) DNA nanotechnology: From sensing and DNA machines to drug-delivery systems. *ACS Nano* 7:8320–8332.
29. Wang S, et al. (2017) Controlling the catalytic functions of DNAzymes within constitutional dynamic networks of DNA nanostructures. *J Am Chem Soc* 139:9662–9671.
30. Wang S, et al. (2018) Light-induced reversible reconfiguration of DNA-based constitutional dynamic networks: Application to switchable catalysis. *Angew Chem Int Ed Engl* 57:8105–8109.
31. Yue L, et al. (2018) Intercommunication of DNA-based constitutional dynamic networks. *J Am Chem Soc* 140:8721–8731.